Organic Selenium induces ferroptosis in pancreatic cancer cells

Roberta Noè [a,b,1], Noemi Inglese [a,b,1], Patrizia Romani [c,1], Thauan Serafini [a], Carlotta Paoli [a,b], Beatrice Calciolari [a,b], Marco Fantuz [a,b], Agata Zamborlin [d,e], Nicoletta C. Surdo [a,g], Vittoria Spada [a], Martina Spacci [a,b], Sara Volta [a], Maria Laura Ermini [e], Giulietta Di Benedetto [a,g], Valentina Frusca [e,f], Claudio Santi [h], Konstantinos Lefkimmiatis [a,i], Sirio Dupont [c], Valerio Voliani [e,j,**], Luca Sancineto [h,***], Alessandro Carrer [a,b,*]

[a] *Veneto Institute of Molecular Medicine (VIMM), 35129, Padova, Italy*
[b] *Department of Biology, University of Padova, 35126, Padova, Italy*
[c] *Department of Molecular Medicine, University of Padova, 35126, Padova, Italy*
[d] *NEST-Scuola Normale Superiore, 56127, Pisa, Italy*
[e] *Center for Nanotechnology Innovation, Istituto Italiano di Tecnologia, 56127, Pisa, Italy*
[f] *Scuola Superiore Sant'Anna, Piazza Martiri della Libertà 33, 56127, Pisa, Italy*
[g] *Neuroscience Institute, National Research Council (CNR), 35121, Padova, Italy*
[h] *Group of Catalysis and Green Organic Chemistry, Department of Pharmaceutical Sciences, University of Perugia, 06122, Perugia, PG, Italy*
[i] *Department of Molecular Medicine, University of Pavia, Pavia, Italy*
[j] *Department of Pharmacy, School of Medical and Pharmaceutical Sciences, University of Genova, 16148, Genoa, Italy*

ARTICLE INFO

ABSTRACT

Pancreatic ductal adenocarcinoma (PDA) cells reprogram both mitochondrial and lysosomal functions to support growth. At the same time, this causes significant dishomeostasis of free radicals. While this is compensated by the upregulation of detoxification mechanisms, it also represents a potential vulnerability.

Here we demonstrate that PDA cells are sensitive to the inhibition of the mevalonate pathway (MVP), which supports the biosynthesis of critical antioxidant intermediates and protect from ferroptosis. We attacked the susceptibility of PDA cells to ferroptotic death with selenorganic compounds, including dibenzyl diselenide (DBDS) that exhibits potent pro-oxidant properties and inhibits tumor growth *in vitro* and *in vivo*. DBDS treatment induces the mobilization of iron from mitochondria enabling uncontrolled lipid peroxidation. Finally, we showed that DBDS and statins act synergistically to promote ferroptosis and provide evidence that combined treatment is a viable strategy to combat PDA.

1. Introduction

Pancreatic ductal adenocarcinoma (PDA) is an aggressive malignancy typically diagnosed at late stages when therapeutic options are inefficacious. PDA cells are characterized by several metabolic disturbances that lead to elevation of reactive oxygen species (ROS) [1]. While this promotes carcinogenesis through multiple mechanisms, including cysteine/methionine oxidation [2,3], genomic instability [4] and altered stromal interactions [5], cancer cells carefully control ROS levels to avoid the accumulation of toxic species.

Refractoriness to cell death is a well-recognized hallmark of cancer that contributes to tumorigenesis and to therapy resistance [6]. Cumulating evidence indicates that ROS signaling can dictate sensitivity to non-apoptotic forms of programmed cell death, such as necroptosis and ferroptosis [7].

Necroptosis is triggered by diverse cues that converge on the activation of Receptor-Interacting Protein Kinase 1/3 (RIPK1, RIPK3) and assembly of effector complex (necrosome) that induces membrane permeabilization [8]. Perhaps counterintuitively, necroptosis supports pancreatic carcinogenesis in mice [9] and promotes cell migration [10]

indicating heterogeneous contribution to PDA pathology [11,12].

Ferroptosis is driven by a chain of Fenton reactions (iron- and oxygen radicals-mediated) that generate toxic phospholipid hydroxyperoxides on cell membranes [13,14]. A variety of cellular systems dictate the balance between accumulation of these noxious radicals and their detoxification in normal, unperturbed cells [14]. In contrast, PDA cells rewire organelle function leading to significant increase of both iron availability and ROS production [15–18]. This increases cell-intrinsic susceptibility to ferroptotic death that is quenched by a variety of antioxidant mechanisms unless environmental cues destabilize defense systems [19]. Among those, the most critical role is played by glutathione peroxidase 4 (GPX4), a selenocysteine-containing protein (selenoprotein) that detoxifies peroxidated lipids using reduced Glutathione (GSH) as co-factor [20]. Thanks to the apparent lack of transcriptional regulation, it can be harnessed for cancer therapy although efficacy remains variable and toxicity elevated [19,21]. In fact, inducing ferroptosis has been shown to inhibit PDA growth *in vitro* and *in vivo* [22–24] although opposite effects have been also reported [25,26]. There is hot demand for a better understanding of the molecular events that determine susceptibility to ferroptotic death as well as for the development of novel chemical inducers.

In living organisms, selenium (Se) is a trace element that can be incorporated in cysteines in spite of sulfur, generating selenocysteine. Only 25 selenoproteins have been identified in humans and most of them are involved in redox stabilization, in part because of the unique biochemical properties of their seleno group [27,28]. These very same properties can be exploited for the rational design of selenorganic compounds with unique redox-modifying potential [29,30]. Intriguingly, these can be easily synthetized but their impact on cell biology and their effective applicability in medicinal chemistry is unclear and still under debate [31].

Selenium uptake and metabolism impact ferroptosis susceptibility [32–36]. More in general, cellular metabolism pathways participates in the defense against ROS-associated ferroptosis [21,37]. Among these, the mevalonate pathway (MVP) is upregulated in PDA [38] and generates a number of radical-trapping isoprenoids that mitigate oxidative stress [21,37].

The rate-limiting enzyme in the MVP is targeted by a class of highly selective drugs called *statins*. The anti-neoplastic properties of statins are still unclear, despite widespread use [39]. Simvastatin treatment in PDA cells reduces the abundance of the MVP-derived Coenzyme Q (CoQ), an electron-shuttling co-factor, and elicits the production of reactive oxygen species (ROS) [40]. Hence, statins clearly interfere with the ferroptotic regulatory penumbra and can induce ferroptosis [14,41–44]. However, statin consumption shows negligible benefit for cancer patients and is insufficient to trigger therapeutically-relevant tumor cell death *in vivo*.

Here, we expand on previous findings and demonstrate that statin treatment unleashes ROS elevation in PDA cells and promotes death by ferroptosis. We then characterized an organic seleno compound, dibenzyl diselenide (DBDS) as a ferroptotic inducer able to suppress PDA growth both *in vitro* and *in vivo*. Mechanistically, DBDS impairs mitochondrial structure and function, also liberating organelle-buffered iron. We strategically combined MVP targeting and DBDS administration to attack both the core and regulatory cellular systems that dictate sensitivity to ferroptosis. Our data point to a synergistic effect between DBDS and statin treatment.

2. Material and methods

Cell lines. All PDA cell lines were cultured in DMEM supplemented with 10 % Fetal Bovine Serum (FBS) (Biowest, S1810) supplemented with 0.3 mg/mL Glutamine. Human pancreatic duct epithelial cells (HPDE) were kindly donated by R. Perera (UCSF, USA) and cultured in RPMI medium supplemented with 10 % FBS. Panc1 were kindly provided by I. Szabó (University of Padova); MiaPaca-2, AsPC1 were kindly

provided by V. Corbo (University of Verona); KP4 were donated by R. Zoncu (UC Berkeley, USA).

Cell lines in the lab have been authenticated by short tandem repeat (STR) profiling using the Geneprint® 10 System (Promega). Data were matched against the ATCC reference database. All cell lines were matched to their identity with a score >80 %.

Primary KPCY-derived cells were described in Ref. [45] and purchased from Krasfast Inc. (Boston, USA): KPCY 6419c5 (#EUP005), KPCY 2838c3 (#EUP013).

Reagents. The following <u>inhibitors</u> were used (concentration, unless otherwise indicated): simvastatin (TargetMol, T0687, 20 μM), ferrostatin-1 (Merck SML0583, 2 μM). The following <u>supplements</u> were used at concentrations indicated in figure legends: mevalonate (Merck, 94259, 500 μM), farnesyl pyrophosphate (Merck #F6892, 100 μM) isopentenyl pyrophosphate (Merck #F6892, 100 μM), isopentenyl pyrophosphate (Merck #I0503, 100 μM), geranylgeranyl pyrophosphate (Merck #G6025, 100 μM), squalene (Merck, S3626, 15-30 μM), Coenzyme Q (Merck C9538, 15 μM).

The following antibodies were used for immunofluorescence: anti-4HNE (Ab48506; 1:250) anti-TOMM20 (GTX 133756; 1:400).

Synthesis of selenium organic compounds. Diphenyl diselenide (DPDS), Diphenylselenide (DPS) and Phenylseleninic acid (PSA) were purchased from Sigma Aldrich and used without further purifications. Dibenzyl diselenide (DBDS) and 2,2′-diselanediyldibenzoic acid (DSBA) were prepared as reported [46]. Ebselen was prepared as reported in Ref. [47]; PhSeZnCl was prepared as reported in Ref. [48]. All the spectroscopic data of the prepared compounds match those reported in literature.

Compounds named "OL1", "OL2" and "OL3" were newly synthesized by the Sancineto group and their structure and synthesis are protected by a pending patent.

Synthesis of DBDS loaded gold nano architectures (DBDS-NAs). Silica shell was formed with a modified Stöber reaction. The array suspension was added to 70 mL of absolute ethanol (Sigma-Aldrich, 24105) previously supplemented with 40 μL of tetraethyl orthosilicate (TEOS, 98 %, Sigma-Aldrich, 131903) and 2.4 mL of ammonium hydroxide (Sigma-Aldrich, 221228). The mixture was gently shaken at room temperature for 3 h. DBDS-NAs were collected by 30-min centrifugation at 3220 rcf. NAs were washed with ethanol and with Milli-Q® water to discard unreacted precursors. A short spin (14 s at 14462 rcf) was employed to remove the bigger DBDS-NAs, while the supernatant was washed in ethanol and stored in ethanol at −20 °C.

Cell growth and proliferation. Cell growth *in vitro* was measured by manual counting of live cells with Burker chamber, as previously reported [38]. Alternatively, ATPlight assay (Promega) was applied according to manufacturer's instructions. Crystal Violet (Merck #C0775; 0.1 % for 20 min) staining was performed according to manufacturer's instruction.

Cells were pulsed with EdU (5-ethynyl-2′-deoxyuridine) for 1 h, fixed and EdU-containing nuclei were developed and imaged. Percentage of EdU + nuclei (counterstained with DAPI) was measured in each acquired field. Data show average of at least 5 fields/well; three biological replicates per condition.

Fluorescent probes and imaging. The following dyes were added at endpoint: 1 μM DCFDA (2′,7′–dichlorofluorescein diacetate, Merck, D6883) for 10 min; 1 μM of MitoSOX™ Red reagent (Life Technologies, M36007) 10 min; 5 μM C11-BODIPY-581/591 (Thermo, D3861) 15 min; 100 nM of Image-iT™ TMRM Reagent (Thermo, I34361) 15 min; 5 μM of Mito-FerroGreen (Dojindo Molecular Technologies, M489) 30 min; 1 μM of BioTracker™ FerroOrange Live Cell Dye (Merck, SCT210) 30 min. For the examination of propidium iodide incorporation, 2 μg/ml of propidium iodide solution in water (Life Technologies, P3566) was added at time 0 to the cells. Staining was carried out in cells plated on 8 multi-well chamber (Ibidi, 80806).

The following dyes were added before the treatments with simvastatin and DBDS:1 μM of Liperfluo (Dojindo Molecular Technologies,

L248-10) for 30 min; 1 μM of BioTracker™ FerroOrange Live Cell Dye (Merck, SCT210) for 30 min.

For image acquisition, cells were placed in the temperature (37 °C)-controlled coverslip holder of a Leica Stellaris confocal microscope equipped with a charge-coupled camera. For multichannel acquisitions, a main beam splitter 405/488/555/639 was used.

Images were analyzed by using a protocol for automatization analysis with the Columbus software. Cytoplasmic and mitochondrial ROS in the cells were calculated as a ratio between the mean fluorescence intensity and the area of each cell. Lipid peroxidation was calculated as a ratio between non-oxidized C11 (591 nm, red) and oxidized C11 (510 nm, green) for each cell. *Immunofluorescence*

PANC-1 and KP4 cells were seeded on round microscopes glass slides, treated as indicated and then stained. Cells were fixed with 4 % paraformaldehyde for 15 min and permeabilized with 0.1 % TritonX/PBS for 10 min at room temperature.

Primary antibodies were incubated overnight at 4° in blocking solution. Secondary antibodies (Jackson ImmunoResearch) were incubated in blocking solution for 1 h at RT. As the final step nuclei were counterstained with Hoechst 33342 for 15 min at room temperature and the slides were mounted with the ProLong Glass mountant (Invitrogen, P36982). Cells were immediately imaged by confocal microscopy.

GSH quantification assay. KP4 cells were treated with 10 μM of DBDS for 10 min and the Glutathione Assay Kit (GSH, GSSG and Total) (amsbio, K6264-100) was used according to manufacturer's instructions.

Cell toxicity assay. Cells were treated as indicated and toxicity was evaluated using Promega's CellTox® assay per manufacturer's instructions.

IC50 calculation. The half maximal inhibitory concentration (IC50) was measured at decreasing concentrations of DBDS using Crystal Violet. Cells were seeded at low density, treated with indicated concentrations of DBDS the day after and stained with Crystal Violet after additional two days. The dye was solubilized and absorbance quantified as a measure of cell viability upon treatment. Data were analyzed and plotted using GraphPad Prism™.

Tumor xenografts. C57BL/6J mice were injected subcutaneously (2.5 $\times 10^5$ cells/mouse) with both KPCY 2838c3 and KPCY 6419c5 (Kerafast™) in contralateral flanks. When tumors became palpable, mice were treated with DBDS (1 mg/kg or 100 μg/kg, i.p) three times/week, simvastatin (10 mg/kg, i.p) five times/week or vehicle (1 % DMSO). Tumor volume was evaluated every other day using calipers and expressed in mm^3 using the formula: V = π/6 × (Dmax^2 × Dmin/2).

Flow cytometry. AnnexinV-FITC/PI apoptosis detection kit (Canvax CA011) was used according to manufacturer's instructions. Staining for ROS uptake, ferroptosis and iron detection were carried out by incubating cells in plates with the indicated reagents in medium without phenol red: 1 μM DCFDA, 1 μM MitoSOX, 5 μM C11-BODIPY-581/591, 1 μM FerroOrange Live Cell Dye and 5 μM of LiperFluo. BD Canto-CALIBUR was for acquisition and analysis. Cells were gated based on SSC-A or FSC-A to eliminate cell debris and on SSC-A to eliminate cell doublets. The median fluorescence intensity was measured for each independent biological sample based on at least 3×10^4 gated events. For C11-BODIPY-581/591, the signals from both non-oxidized C11 (PE–A) and oxidized C11 (FITC-A) were acquired, and ratio of medians (FITC-A to PE–A) was calculated for each sample.

Metals quantification using Inductively Coupled Plasma-Mass Spectrometry (ICP-MS). Cell pellets and organs from DMSO- or DBDS-injected mice were dried at 80 °C. Upon transfer into 10 mL-pressured vials, samples were digested at 100 °C using *aqua regia* made of 3:1 hydrochloric acid (34–37 % in HCl; TraceMetal Grade, Thermo Fisher Scientific, #A508-P500) and nitric acid (65 % Suprapur®; Sigma-Aldrich, #1.00441). When dried, 2.5 mL of 3 % nitric acid solution was used to dilute the samples that were run into ICP-MS. Metal content in cell pellets and organs was quantified by analysis against standard calibration curves (Selenium and Iron standard 10 ppm, TraceCERT® Periodic

table mix 1 for ICP, Sigma-Aldrich, #92091), using 10 ppm Hg (10000 ppm; Sigma-Aldrich, #75111) in 3 % nitric acid solution as internal standard.

Western blotting. For immunoblotting cells were lysed in lysis buffer (25 mM Tris-HCl pH7.4, 150 mM NaCl, 1 mM EDTA, 5 % glycerol, 1 % NP-40), supplemented with PhosSTOP phosphatase inhibitor cocktail (Roche) and protease inhibitor cocktail (Roche). 50 μg of protein per sample were resolved on 10 % SDS-Urea PAGE gel and transferred to PVDF membranes. Membranes were blocked in 10 % milk for 1h at room temperature. Incubation with the appropriate dilution of primary antibody was carried out at 4 °C o/n. RIPK1 (BD Transduction Laboratories, Cat#610459, 1:1000), RIPK3 (Cell signaling, Cat#13526S, 1:1000). Horseradish peroxidase conjugated secondary antibodies were used at a dilution of 1:5000. Loading control antibody β-actin HRP-conjugated (Sigma-Aldrich, Cat# A3854, 1:4000) was incubate for 45 min at room temperature.

Generation of RIPK3-deficient cells. Two 21 bp single guide sequences targeting the second exon of the human RIPK3 gene (ENSG00000129465) were designed using CRISPRdirect (https://crispr.dbcls.jp/). Sequences:

Crispr_RIPK3_232: 5′-CACCGAACCAGGAGCTCGTCGGCAA-3'
Crispr_RIPK3_232 compl: 5′-AAACTTGCCGACGAGCTCCTGGTTC-3'
Crispr_RIPK3_274: 5′-CACCGCGGGCGCAACATAGGAAGTG -3'
Crispr_RIPK3_274 compl: 5′-AAACCACTTCCTATGTTGCGCCCGC-3'

The oligonucleotides were then phosphorylated with T4 polynucleotide kinase, annealed and cloned in the BbsI-digested px458 plasmid (pSpCas9(BB)-2A-GFP, Addgene #48138). Constructs were verified by sequencing and employed to co-transfect HT29 cells. Twenty-four hours after transfection EGFP-expressing cells were FACS sorted and isolated clones were amplified. The Cas9 cleavage efficiency of the RIPK3 gene in the selected clones has been verified by Western blot.

Statistical Analysis. Data are presented as the means of experimental replicates with their respective standard deviations (SD), unless otherwise indicated. For cell number quantifications, Student two-tailed t tests (two-sample equal variance, two-tailed distribution) were used for analyses, unless otherwise indicated. Repeated-measures ANOVA with Tukey–Kramer adjustment for multiple comparisons was used to evaluate significant differences in tumor growth. For survival, log-rank test was performed using GraphPad Prism. For quantifications of fluorescence intensities in cell populations, one-way ANOVA was used. Significance was defined as follows: *, P < 0.05; **, P < 0.01; ***, P < 0.001.

3. Results

Consistent with our previous findings [38], PDA cell growth *in vitro* is sensitive to statins (e.g.: *simvastatin*) while supplementation with mevalonate rescues cell number after treatment (Suppl. Figs. 1A–C). These data point to a pro-survival role of MVP intermediates downstream HMGCR and are in line with a growing body of evidence [49,50].

3.1. Mevalonate pathway inhibition induces ferroptosis

Multiple intermediates downstream of mevalonate are known to stabilize redox stress (Suppl. Fig. 1B, highlighted in color bold). Hence, we tested ROS production in statin-treated PDA cells. We found that simvastatin massively induces both cytoplasmic and mitochondrial redox species (Fig. 1A–B; Suppl. Fig. 1D), while mevalonate addition completely suppresses ROS elevation (Fig. 1D). These findings suggest that the mevalonate pathway is sustained in PDA to keep ROS levels in check.

Deregulation of MVP intermediates sensitizes cancer cell to ferroptosis [21]. In line, simvastatin-treated PDA cells exhibit a strong increase of peroxidated lipid species, normalized by supplementation with mevalonate and CoQ (Fig. 1C–S; Suppl. Figs. 1E–F). Similarly, levels of
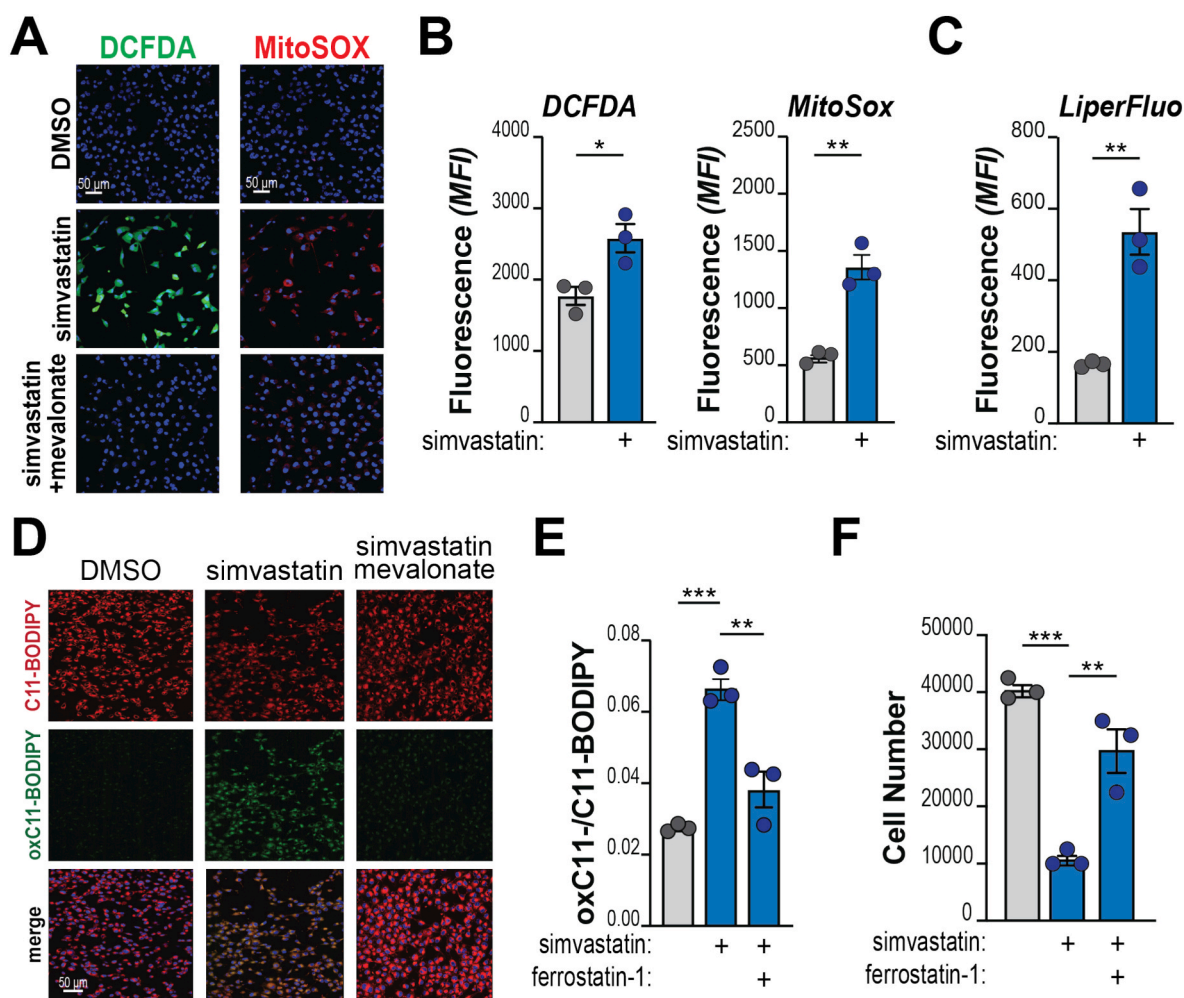
Fig. 1. Inhibition of the mevalonate pathway triggers oxidative stress and ferroptosis in PDA. A, KP4 cells were treated with simvastatin (20 μM) w/or w/o supplementation with mevalonate (500 μM) for 2 h and stained for the detection of cytoplasmic (DCFDA, green) or mitochondrial (MitoSOX, red) ROS. Nuclei counterstained with HOECHST. Representative images (quantification in Suppl. Fig. 1). **B–C,** Flow cytometry analysis of KP4 treated with simvastatin (20 μM) showing enhanced ROS (**B**) and lipid peroxides (**C**) levels. **D,** KP4 cells were treated with simvastatin (20 μM) w/or w/o supplementation with mevalonate (500 μM) and incubated with C11-BODIPY after 1 h. Representative images of split channels (red: reduced C11; green: oxidized C11) and merge. **E-F,** KP4 cells were treated with simvastatin (20 μM) and/or Ferrostatin-1 (2 μM) and stained with C11-BODIPY (**E**). Graph shows the ratio between oxidized and reduced C11, quantified by flow cytometry (ratio of mean fluorescence intensity (MFI) for each sample). In **F,** cells were counted after 2 days. For all panels, experiments are representative of 2 independent biological repeats. Dots denote biological replicates. Bars show mean, ±SD (*, P < 0.05; **, P < 0.01; ***, P < 0.001; calculated over vehicle-treated cells unless otherwise indicated). (For interpretation of the references to color in this figure legend, the reader is referred to the Web version of this article.)

lipid peroxides were normalized by addition of Ferrostatin-1 (Fer-1), a selective inhibitor of ferroptosis [51] (Fig. 1E) also able to improve cell viability of simvastatin-treated cells (Fig. 1F).

These data support the hypothesis that PDA cells sustain the synthesis of sterol intermediates that collectively dampen cell-intrinsic oxidative stress.

3.2. Organic seleno compounds show anti-neoplastic properties in vitro

We set out to find novel molecules able to induce ROS and ferroptosis in PDA. To this goal, we decided to interrogate a panel of organic seleno compounds to exploit and maximize the intriguing biochemical properties of selenium. We screened molecules that contain highly diverse heterogeneous functional groups, including selenides, diselenides and one seleninic acid (Suppl. Fig. 2A). Each compound was added to *in vitro* cultures of primary cells derived from autochthonous murine tumors (*Pdx1-Cre;LSL-Trp53^{fl/fl};LSL-KrasG12D^{fl/fl}*; hereafter, *KPC* cells). We found that diselenides and seleninic organic acids potently suppress cell growth *in vitro* (Fig. 2A). Dibenzyl diselenide (DBDS) showed the most potent inhibition across murine and human cell lines (KPC and Panc1,

respectively; Fig. 2B). When compared to Ebselen, which is in phase II/III clinical testing for infectious and auto-immune diseases, or newly-synthesized PhSeZnCl [52], DBDS showed superior ability to reduce tumor cell growth (Fig. 2C; Suppl. Figs. 2B–C). Time lapse examination of propidium iodide incorporation revealed the ability of DBDS to induce cell death rapidly (<5 min, peak at 60 min; Suppl. Fig. 2D). Interestingly, this is not linked to altered intracellular availability of selenium because the addition of inorganic selenium at low micromolar concentrations did not inhibit – but rather promoted – cell growth (Suppl. Fig. 2E).

An attractive pharmacological property of DBDS is its ability to be loaded into composite nano-architectures (DBDS-NAs) for efficient drug delivery. NAs are hybrid ultrasmall-in-nano architectures that comprise metal (Au-based) ultrasmall nanoparticles (3 nm) within a polymeric matrix shielded by a silica shell [53]. NAs are highly versatile nano-platforms with a convenient biokinetics to avoid metal persistence after intranasal or intravenous administration [53,54]. Drugs can be included in the inner core of NAs to protect them from the physiological environment and improve their delivery to the target [55]. In this regard, DBDS was included in NAs without affecting their morphological
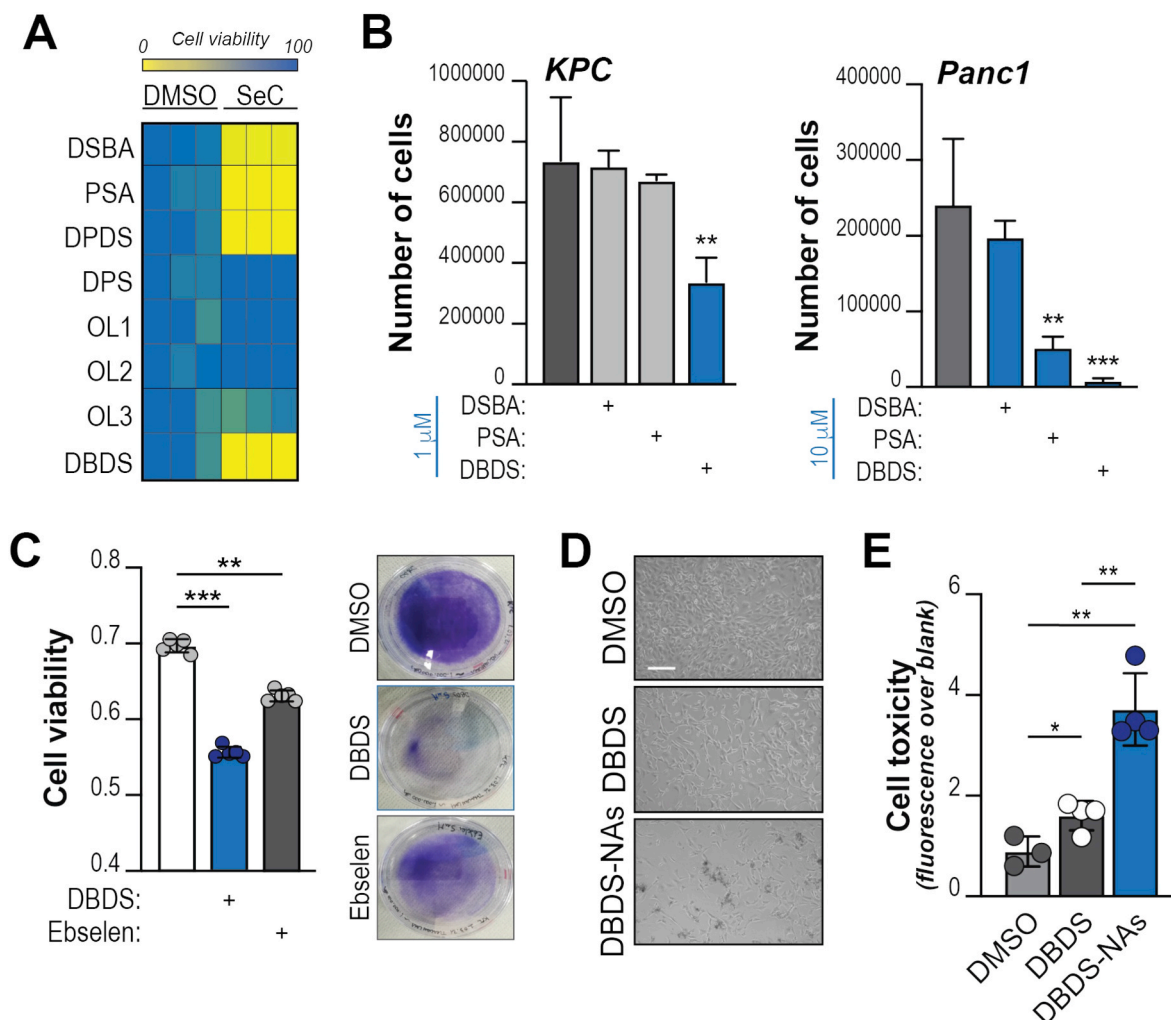
Fig. 2. Dibenzyl diselenide is an anti-neoplastic compound. A, Indicated selenocompounds (SeC) were administered to KPC cells (100 μM). The heatmap shows percentage of growth relative to vehicle (DMSO)-treated cells (for each treatment, 100 %). DSBA: 2′,2′-diselanediyldibenzoic acid; PSA: phenylseleninic acid; DPDS: diphenyl diselenide; DPS: diphenylselenide; OL1: patented compound 1; OL2: patented compound 2; OL3: patented compound 3; DBDS: dibenzyl diselenide. **B,** KPC or Panc1 cells were treated with indicated compounds (1 μM and 10 μM, respectively) and counted after 3 days. **C,** KPC cells were treated with indicated compounds and stained with Crystal Violet after 2 days. Right, representative images of culture plates after staining. Left, quantification of solubilized dye; cell viability expressed as absorbance (blank subtracted). **D,** KPC cells were treated with DBDS or DBDS-loaded NAs (for both, final drug concentration: 1 μM). Representative images after 3 days. Scale bar: 100 μm. **E,** KPC cells were treated as in **D** and CellTox® assay was performed at endpoint. Experiments are representative of 2 independent biological repeats. Dots denote experimental replicates. For **B-E**, bars show mean, ±SD (*, P < 0.05; **, P < 0.01; ***, P < 0.001; calculated over vehicle-treated cells unless otherwise indicated). (For interpretation of the references to color in this figure legend, the reader is referred to the Web version of this article.)

features as demonstrated by Transmission Electron Microscopy (TEM) images (diameter: 174 ± 77 nm). Inductively coupled plasma-mass spectrometry (ICP-MS) reported a mols ratio of Se/Au of 12 %, which equates to a DBDS/Au mols ratio of 6 %. Interestingly, NAs-loaded DBDS significantly reduce cell viability compared to low dose free DBDS (Fig. 2D–E; Supp. Fig. 2F).

Collectively, these results point to DBDS as an attractive molecule with a potent, yet poorly characterized anti-neoplastic activity.
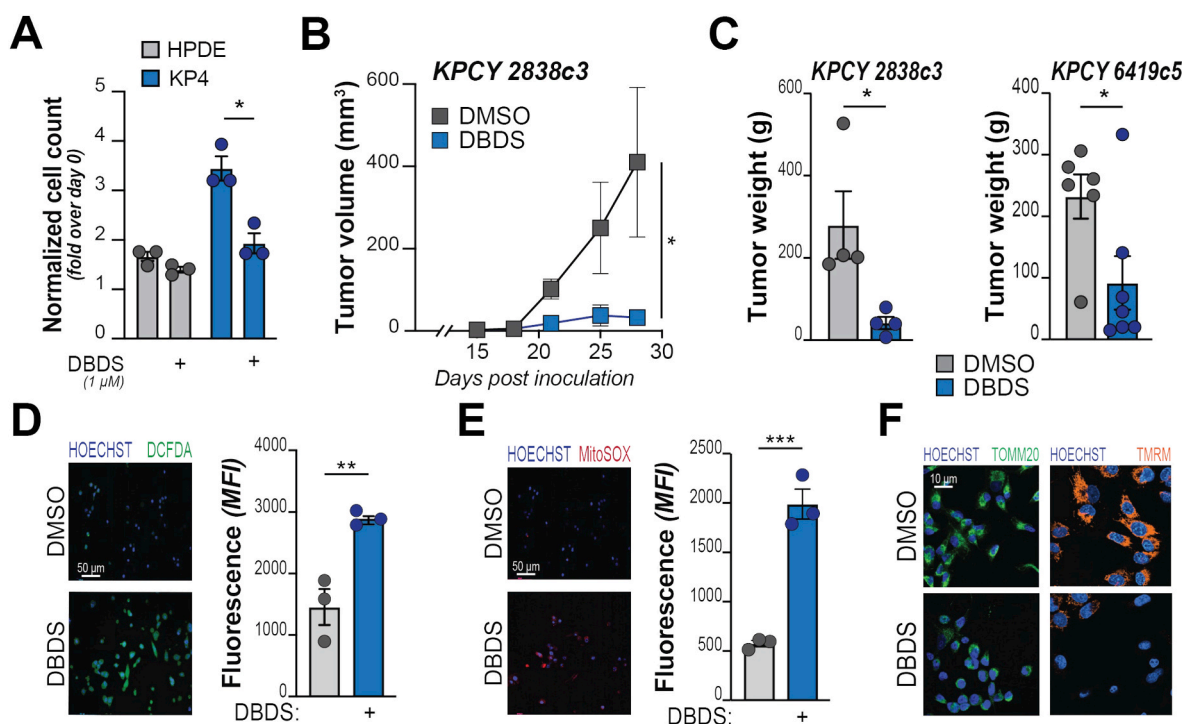
3.3. DBDS inhibits tumor growth

To test the impact of DBDS on non-transformed cells, we compared cell viability upon DBDS administration to either Human Pancreatic Duct Epithelial (HPDE; primary from normal ducts) or human PDA (KP4; tumor-derived) cell lines. We found that HPDE are negligibly affected by DBDS at a dose that significantly reduces the viability of KP4 *in vitro* (Fig. 3A). Importantly, treatment with DBDS alone decreases the growth of PDA tumor xenografts *in vivo* (Fig. 3B–C; Suppl. Fig. 3A). DBDS administration at 1 mg/kg (3x/week) is well tolerated in mice that

exhibit no signs of distress and a peak DBDS level of 0.9 μg per mL of blood.

Mechanistically, DBDS did not alter the proliferation of PDA cells (Suppl. Fig. 3B) but led to the rapid (<1 h) generation of ROS, which accumulate in both the cytoplasm (Fig. 3D; Suppl. Fig. 3C) and mitochondria (Fig. 3E; Suppl. Fig. 3D). We also found that DBDS induces sudden collapse of mitochondria that quickly acquire highly fragmented phenotype, convolute toward the nuclear periphery and exhibit signs of impaired activity (Fig. 3F; Suppl. Fig. 3D). The breakdown of mitochondria shape and function likely explains the remarkable elevation of mitochondria-derived radicals.

3.4. DBDS induces ferroptosis in PDA cells

We hypothesized that DBDS might trigger a deregulation of redox balance that impairs cell fitness. Cell treated with DBDS rapidly die (Suppl. Fig. 2D). To get insight into the mechanisms responsible for DBDS-induced cell death, we performed propidium iodide/Annexin V co-staining that showed absence of apoptotic cells upon treatment with

Fig. 3. DBDS elicits oxidative stress and inhibits tumor growth. A, Indicated cell lines (non-transformed: grey bars; PDA: blue bars) were treated with DBDS (1 μM) and counted after 2 days. Bars show increase of cell number (over cells counted at day 0 – pre-treatment). **B–C,** KPCY-derived tumor cell clones (2838c3 or 6419c5) were implanted subcutaneously into immune-competent C57BL/6J mice and treated with either DBDS (1 mg/kg) or vehicle (DMSO 1 %), three times per week after tumors became palpable (day 15 after inoculation). Tumor size (**B**) was monitored during the experiment; tumor weight (**C**) documented at end point. **D-E,** PDA cells were treated with DBDS (10 μM) and stained for the detection of cytoplasmic (DCFDA, in **D**) or mitochondrial (MitoSOX, in **E**) ROS. For each panel, representative images are shown on the left; FACS quantification on the right. F, KP4 cells were treated with DBDS (10 μM) and mitochondrial network morphology (green, left panels, showing outer membrane protein TOMM20) or polarization (orange, right panels, showing emission of TMRM) assessed by imaging. For **A, C, D, E** bars show mean, ±SD; dots denote biological replicates. For **B**, squares indicate mean ± SD at indicated time points. For all panels, *, P < 0.05; **, P < 0.01; ***, P < 0.001; calculated over vehicle-treated cells unless otherwise indicated. (For interpretation of the references to color in this figure legend, the reader is referred to the Web version of this article.)

DBDS (Suppl. Fig. 4A). We thus interrogated forms of non-canonical cell death, focusing on necroptosis and ferroptosis that are ROS-sensitive and have been described in multiple tumors, while pyroptosis is thought to be mostly limited to the immune compartment [56]. Interestingly, most PDA cells negligibly express the key necroptotic effector RIPK3 (*data not shown*); this observation suggests that necroptosis is likely not responsible for DBDS induced cell death. Nevertheless, we tested the impact of DBDS administration on the viability of colon cancer cell clones where *RIPK3* had been genetically ablated. DBDS reduced cell growth of both the parental cell line (HT29) and HT29 *RIPK3*-KO cells (Suppl. Fig. 4B), further indicating that DBDS drives non-necroptotic cell death. Of note, RIPK3-deficient cells showed enhanced sensitivity, in line with previous findings in *Ripk3*-mutant mice that exhibit hyper-sensitivity to ferroptotic death [57].

To test whether DBDS-induced oxidative stress leads to ferroptotic death, we examined and quantified the peroxidation of membrane lipids in PDA cells using C11-BODIPY. We observed a dose-dependent red-to-green fluorescence shift upon DBDS treatment, which was prevented by co-treatment with either Ferrostatin-1 or the anti-oxidant N-acetyl-cysteine (NAC) (Fig. 4A; Suppl. Fig. 4C). In addition, we observed a significant accumulation of 4-hydroxynonenal (4-HNE), a toxic byproduct of lipid peroxides (Suppl. Fig. 4D) and augmented lipid per-oxidation was also detected by a specific fluorescent probe – LiperFluo (Suppl. Fig. 4E). Supplementation with Ferrostatin-1 could restore viability of DBDS-treated cells (Fig. 4B). Together, these data indicate that DBDS administration elicits ferroptosis in PDA.

A distinctive feature of ferroptosis is the requirement for labile iron to drive radical-mediated attack to membrane lipids. In fact, DBDS in-duces significant elevation of Fe2+ availability (Fig. 4C) without

changes in the balance between reduced and oxidized glutathione (GSH: GSSG; Fig. 4D), which mediates primary defense against lipid peroxi-dation. Similarly, GPX4 levels were not affected (*data not shown*). Our data suggest that DBDS perturbs the integrity of mitochondria (Fig. 3F) that buffer intracellular iron availability [58,59]. In fact, we observed that DBDS administration elevated organelle-confined iron (Suppl. Fig. 4F). This is likely liberated from Fe–S clusters or accumulates due to halted heme biosynthesis.

While statins can induce ferroptosis targeting the cell's "regulatory penumbra" [14], DBDS directly attacks the core mechanisms that trigger ferroptosis. Because the two compounds operate at opposite edges of a complex biochemical spectrum, we anticipated that the combined treatment of DBDS and simvastatin could have an additive – and perhaps synergistic – effect on cell death. Indeed, combo administration syner-gistically led to lower cell viability *in vitro* (Fig. 4E) and to a significant reduction of tumor growth *in vivo* (Fig. 4F).

Our findings in PDA cells point to diselenides as novel ferroptosis inducers and to MVP intermediates as critical ferroptosis-shielding antioxidants.

4. Conclusions

The metabolic makeup of PDA predisposes cancer cells to ferroptosis, which is gaining interest as an actionable process that might selectively kill cancer cells [60,61]. Increased iron bioavailability [16], mitochon-drial remodeling [62] and enhanced activity [63], sustained lipid scavenging [64] are all distinctive features of PDA and together contribute to elevated levels of lipid peroxidation [14].

Building from prior investigations [38], we speculated that PDA cells
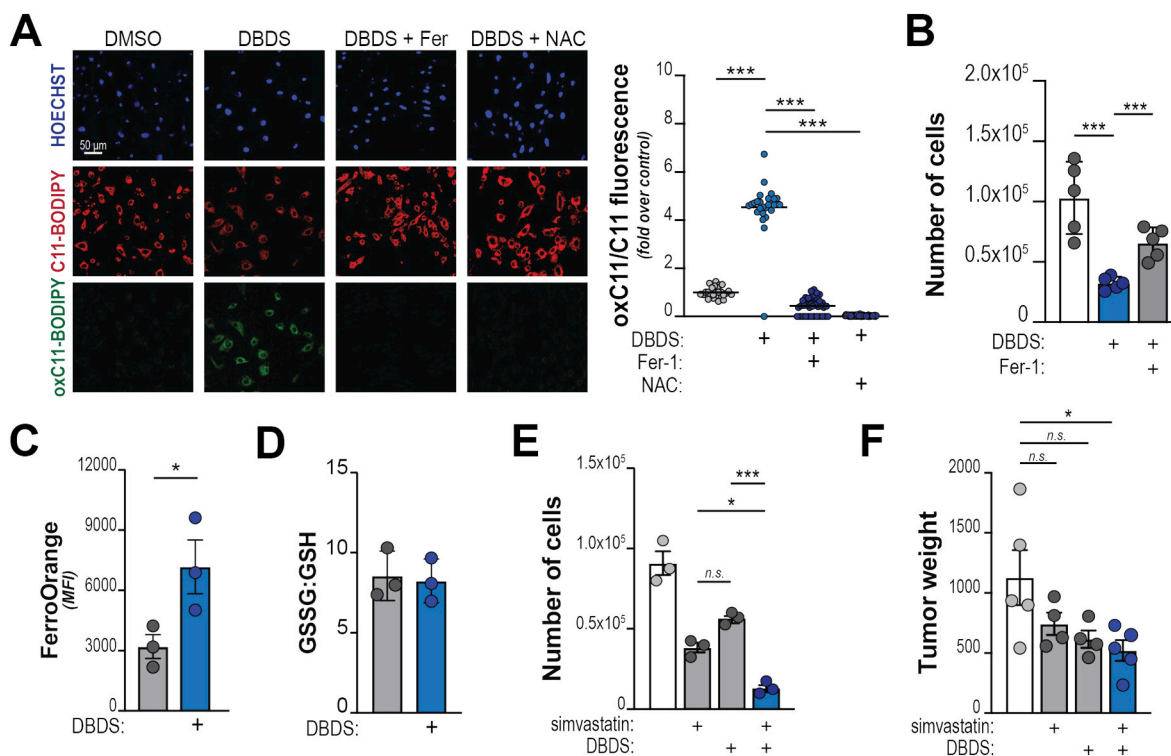
Fig. 4. DBDS is a ferroptosis inducer. A, KP4 cells were treated with DBDS (10 μM) w/or w/o supplementation with Ferrostatin-1 (Fer-1; 2 μM) or N-acetyl-cysteine (NAC; 10 μM) and incubated with C11-BODIPY for 15. Left, representative images. Right, quantification of red-to-green (indicative of lipid peroxidation) fluorescence shift. **B,** KP4 cells were treated with DBDS (5 μM) w/or w/o Ferrostatin-1 (2 μM) and counted after 2 days. **C-D,** KP4 cells were treated with DBDS (10 μM). **C** shows whole-cell iron abundance, quantified by flow cytometry (FerroOrange staining); **D** shows relative levels of GSH and GSSG levels. **E,** KP4 cells were treated with simvastatin (5 μM) and/or DBDS (1 μM) and cell viability examined after 2 days. **F,** 6419c5 cells were implanted subcutaneously into immune-competent C57BL/6J mice and treated with either DBDS (100 μg/kg) or simvastatin (10 mg/kg), or both, and tumor weight recorded at end point. For **B, C, D, E, F,** bars show mean, ±SD. For **A,** lines show mean, ±95 % CI. For all panels, dots denote experimental replicates. (*, $P < 0.05$; **, $P < 0.01$; ***, $P < 0.001$). (For interpretation of the references to color in this figure legend, the reader is referred to the Web version of this article.)

upregulate the mevalonate pathway (MVP) to quench tumorigenesis-associated oxidative stress and escape ferroptosis. In fact, multiple MVP intermediates are redox-stabilizing lipid species. We demonstrated that statins administration elicits oxidative stress and ferroptotic death in multiple PDA cells, in line with results obtained in other tumor types [65–68]. Statins usage inconsistently correlates to cancer outcome – including PDA risk and survival [39] while their administration has modest impact on tumor growth in animal models [38]. This is possibly due to the presence of abundant stromal elements that influence the redox state of the cell [69,70] and might alleviate pro-ferroptotic signals [22,37]. As new strategies are being developed to specifically curtail the massive stromal compartment of PDA tumors, it will be interesting to test the effect of statins in combination with stroma-targeting therapeutics.

In this study, we explored synergism with selenorganic compounds and found that statins and diselenides cooperatively elicit ferroptosis. Despite mounting evidence showing that selenium (Se) possesses unique biological chemistry features and is essential in the regulation of ferroptosis [33], the activity of organic compounds containing Se has not been well characterized. Screening multiple molecules with hetorogeneous functional groups, we now report that dibenzyl diselenide (DBDS) is a potent pro-oxidant and a unique ferroptosis inducer. In fact, DBDS treatment is sufficient to markedly suppress tumor growth both *in vitro* and *in vivo*.

We were able to document DBDS-induced oxidative stress by monitoring both cytoplasmic and mitochondrial ROS. This suggests the intriguing possibility that DBDS might operate at the mitochondrial level; indeed, DBDS administration rapidly induces a stress-like, ferroptosis-associated response where mitochondria acquire a more fragmented morphology and relocate close to the nuclear periphery while their function falters [71,72]. Interestingly, this is associated with increased abundance of mitochondrial Fe2+ that leads – in turn – to elevated levels of labile iron in the whole cell. We reckon that DBDS sensitizes cells to ferroptotic death through the release of iron from mitochondria, where is largely confined for the synthesis of iron-containing prosthetic groups: heme and iron-sulfur (Fe–S) clusters [73]. Mitochondria control intracellular iron abundance and processing [58] and mitochondrial damage has been shown to impair iron homeostasis while promoting non-apoptotic death [43,74,75]. We report that a similar mechanism applies to DBDS-induced ferroptosis. Of note, Se groups are highly reactive and can dimerize under particular conditions. Se can replace the sulfur ions of the Fe–S cluster [76] and Se-substituted clusters possess smaller donor strength and significantly reduced activity [77,78]. Together, these observations add to the evidence supporting a role of mitochondria in the induction of ferroptosis [21,24] and suggest the intriguing possibility that certain configurations of organic Se might displace Fe–S clusters.

Selenium displays significant chemical flexibility in biological environments. While commonly known for its anti-oxidant properties, mounting evidence shows bivalent behavior [79]. Our data clearly indicates that selenorganic compounds often promote oxidative stress, although we cannot conclusively determine whether this is due to inherent chemical properties of diselenides or is indirectly caused by the disruption of mitochondria. Alternatively, DBDS might suppress central mechanisms of ROS detoxification. In line, diselenides have been shown to inhibit glutathione-S-transferase (GST) at high concentrations [80, 81] and they also might replace Se atoms in selenoproteins, most notably GPX4. These are intriguing possibilities that were not directly

tested in our work, although GSH and GPX4 levels were not affected by DBDS.

In closing, our work identifies a metabolic vulnerability in PDA cells that can be attacked by a combination of statins, a class of well-tolerated drugs, and diselenides, a family of incompletely characterized molecules with unique chemical features. This proof-of-concept strategy hinges on the intrinsic biochemical plasticity of ferroptosis, fostering its core executors (e.g.: iron availability, ROS) while disrupting regulatory defense systems (radical-trapping isoprenoids). We also uncovered novel properties of Se-containing organic compounds that represent attractive building blocks for the design of novel specific ferroptosis inducers.

Declaration of competing interest

None.

Acknowledgments

Animal experimentation present in the study was conducted according to the guidelines of the Declaration of Helsinki and approved by the Ethics Committee of the Veneto Institute of Molecular Medicine and the Italian Ministry of Health (protocol code 646-2020-PR, approved on July 6th, 2020).

Appendix A. Supplementary data

Supplementary data to this article can be found online at https://doi.org/10.1016/j.redox.2023.102962.

References

[1] E.C. Cheung, K.H. Vousden, The role of ROS in tumour development and progression, Nat. Rev. Cancer 22 (2022) 280–297, https://doi.org/10.1038/s41568-021-00435-0.
[2] D. He, H. Feng, B. Sundberg, J. Yang, J. Powers, A.H. Christian, J.E. Wilkinson, C. Monnin, D. Avizonis, C.J. Thomas, R.A. Friedman, M.D. Kluger, M.A. Hollingsworth, P.M. Grandgenett, K.A. Klute, F.D. Toste, C.J. Chang, I.I.C. Chio, Methionine oxidation activates pyruvate kinase M2 to promote pancreatic cancer metastasis, Mol. Cell. 82 (2022) 3045–3060, https://doi.org/10.1016/j.molcel.2022.06.005, e11.
[3] L. Bar-Peled, E.K. Kemper, R.M. Suciu, E. V Vinogradova, K.M. Backus, B. D. Horning, T.A. Paul, T.-A. Ichu, R.U. Svensson, J. Olucha, M.W. Chang, B.P. Kok, Z. Zhu, N.T. Ihle, M.M. Dix, P. Jiang, M.M. Hayward, E. Saez, R.J. Shaw, B. F. Cravatt, Chemical proteomics identifies druggable vulnerabilities in a genetically defined cancer, Cell 171 (2017) 696–709.e23, https://doi.org/10.1016/j.cell.2017.08.051.
[4] M. Nieborowska-Skorska, P.K. Kopinski, R. Ray, G. Hoser, D. Ngaba, S. Flis, K. Cramer, M.M. Reddy, M. Koptyra, T. Penserga, E. Glodkowska-Mrowka, E. Bolton, T.L. Holyoake, C.J. Eaves, S. Cerny-Reiterer, P. Valent, A. Hochhaus, T. P. Hughes, H. van der Kuip, M. Sattler, W. Wiktor-Jedrzejczak, C. Richardson, A. Dorrance, T. Stoklosa, D.A. Williams, T. Skorski, Rac2-MRC-cIII–generated ROS cause genomic instability in chronic myeloid leukemia stem cells and primitive

[5] P. Romani, N. Nirchio, M. Arboit, V. Barbieri, A. Tosi, F. Michielin, S. Shibuya, T. Benoist, D. Wu, C.C.T. Hindmarch, M. Giomo, A. Urciuolo, F. Giamogante, A. Roveri, P. Chakravarty, M. Montagner, T. Calì, N. Elvassore, S.L. Archer, P. De Coppi, A. Rosato, G. Martello, S. Dupont, Mitochondrial fission links ECM mechanotransduction to metabolic redox homeostasis and metastatic chemotherapy resistance, Nat. Cell Biol. 24 (2022) 168–180, https://doi.org/10.1038/s41556-022-00843-w.
[6] D. Hanahan, R.A. Weinberg, Hallmarks of cancer: the next generation, Cell 144 (2011) 646–674, https://doi.org/10.1016/j.cell.2011.02.013.
[7] L. Galluzzi, J.M. Bravo-San Pedro, G. Kroemer, Organelle-specific initiation of cell death, Nat. Cell Biol. 16 (2014) 728–736, https://doi.org/10.1038/ncb3005.
[8] M. Kist, D. Vucic, Cell death pathways: intricate connections and disease implications, EMBO J. 40 (2021), e106700, https://doi.org/10.15252/embj.2020106700.
[9] L. Seifert, G. Werba, S. Tiwari, N.N. Giao Ly, S. Alothman, D. Alqunaibit, A. Avanzi, R. Barilla, D. Daley, S.H. Greco, A. Torres-Hernandez, M. Pergamo, A. Ochi, C. P. Zambirinis, M. Pansari, M. Rendon, D. Tippens, M. Hundeyin, V.R. Mani, C. Hajdu, D. Engle, G. Miller, The necrosome promotes pancreatic oncogenesis via CXCL1 and Mincle-induced immune suppression, Nature 532 (2016) 245–249, https://doi.org/10.1038/nature17403.
[10] Y. Ando, K. Ohuchida, Y. Otsubo, S. Kibe, S. Takesue, T. Abe, C. Iwamoto, K. Shindo, T. Moriyama, K. Nakata, Y. Miyasaka, Y. Ohtsuka, Y. Oda, M. Nakamura, Necroptosis in pancreatic cancer promotes cancer cell migration and invasion by release of CXCL5, PLoS One 15 (2020), e0228015, https://doi.org/10.1371/journal.pone.0228015.
[11] V. Giansante, G. Stati, S. Sancilio, E. Guerra, S. Alberti, R. Di Pietro, The dual role of necroptosis in pancreatic ductal adenocarcinoma, Int. J. Mol. Sci. 24 (2023), https://doi.org/10.3390/ijms241612633.
[12] X. Chen, H.J. Zeh, R. Kang, G. Kroemer, D. Tang, Cell death in pancreatic cancer: from pathogenesis to therapy, Nat. Rev. Gastroenterol. Hepatol. 18 (2021) 804–823, https://doi.org/10.1038/s41575-021-00486-6.
[13] B.R. Stockwell, J.P. Friedmann Angeli, H. Bayir, A.I. Bush, M. Conrad, S.J. Dixon, S. Fulda, S. Gascón, S.K. Hatzios, V.E. Kagan, K. Noel, X. Jiang, A. Linkermann, M. E. Murphy, M. Overholtzer, A. Oyagi, G.C. Pagnussat, J. Park, Q. Ran, C. S. Rosenfeld, K. Salnikow, D. Tang, F.M. Torti, S. V Torti, S. Toyokuni, K. A. Woerpel, D.D. Zhang, Ferroptosis: a regulated cell death nexus linking metabolism, redox biology, and disease, Cell 171 (2017) 273–285, https://doi.org/10.1016/j.cell.2017.09.021.
[14] S.J. Dixon, D.A. Pratt, Ferroptosis: a flexible constellation of related biochemical mechanisms, Mol. Cell. 83 (2023) 1030–1042, https://doi.org/10.1016/j.molcel.2023.03.005.
[15] I.I.C. Chio, S.M. Jafarnejad, M. Ponz-Sarvise, Y. Park, K. Rivera, W. Palm, J. Wilson, V. Sangar, Y. Hao, D. Öhlund, K. Wright, D. Filippini, E.J. Lee, B. Da Silva, C. Schoepfer, J.E. Wilkinson, J.M. Buscaglia, G.M. DeNicola, H. Tiriac, M. Hammell, H.C. Crawford, E.E. Schmidt, C.B. Thompson, D.J. Pappin, N. Sonenberg, D.A. Tuveson, NRF2 promotes tumor maintenance by modulating mRNA translation in pancreatic cancer, Cell 166 (2016) 963–976, https://doi.org/10.1016/j.cell.2016.06.056.
[16] N. Santana-Codina, M.Q. del Rey, K.S. Kapner, H. Zhang, A. Gikandi, C. Malcolm, C. Poupault, M. Kuljanin, K.M. John, D.E. Biancur, B. Chen, N.K. Das, K.E. Lowder, C.J. Hennessey, W. Huang, A. Yang, Y.M. Shah, J.A. Nowak, A.J. Aguirre, J. D. Mancias, NCOA4-Mediated ferritinophagy is a pancreatic cancer dependency via maintenance of iron bioavailability for iron–sulfur cluster proteins, Cancer Discov. 12 (2022) 2180–2197, https://doi.org/10.1158/2159-8290.CD-22-0043.
[17] M. Ravichandran, J. Hu, C. Cai, N.P. Ward, A. Venida, C. Foakes, M. Kuljanin, A. Yang, C.J. Hennessey, Y. Yang, B.R. Desousa, G. Rademaker, A.A.L. Staes, Z. Cakir, I.H. Jain, A.J. Aguirre, J.D. Mancias, Y. Shen, G.M. DeNicola, R.M. Perera, Coordinated transcriptional and catabolic programs support iron-dependent adaptation to RAS–MAPK pathway inhibition in pancreatic cancer, Cancer Discov. 12 (2022) 2198–2219, https://doi.org/10.1158/2159-8290.CD-22-0044.
[18] F. Chiaradonna, D. Gaglio, M. Vanoni, L. Alberghina, Expression of transforming K-Ras oncogene affects mitochondrial function and morphology in mouse fibroblasts, Biochim. Biophys. Acta Bioenerg. 1757 (2006) 1338–1356, https://doi.org/10.1016/j.bbabio.2006.08.001.
[19] X. Jiang, B.R. Stockwell, M. Conrad, Ferroptosis: mechanisms, biology and role in disease, Nat. Rev. Mol. Cell Biol. 22 (2021) 266–282, https://doi.org/10.1038/s41580-020-00324-8.
[20] M. Maiorino, M. Conrad, F. Ursini, GPx4, lipid peroxidation, and cell death: discoveries, rediscoveries, and open issues, Antioxidants Redox Signal. 29 (2017) 61–74, https://doi.org/10.1089/ars.2017.7115.
[21] J. Zheng, M. Conrad, The metabolic underpinnings of ferroptosis, Cell Metabol. 32 (2020) 920–937, https://doi.org/10.1016/j.cmet.2020.10.011.
[22] M.A. Badgley, D.M. Kremer, H.C. Maurer, K.E. DelGiorno, H.-J. Lee, V. Purohit, I. R. Sagalovskiy, A. Ma, J. Kapilian, C.E.M. Firl, A.R. Decker, S.A. Sastra, C. F. Palermo, L.R. Andrade, P. Sajjakulnukit, L. Zhang, Z.P. Tolstyka, T. Hirschhorn, C. Lamb, T. Liu, W. Gu, E.S. Seeley, E. Stone, G. Georgiou, U. Manor, A. Iuga, G. M. Wahl, B.R. Stockwell, C.A. Lyssiotis, K.P. Olive, Cysteine depletion induces pancreatic tumor ferroptosis in mice, Science 368 (2020) 85–89, https://doi.org/10.1126/science.aaw9872.
[23] Z. Ye, Q. Zhuo, Q. Hu, X. Xu, Mengqi liu, Z. Zhang, W. Xu, W. Liu, G. Fan, Y. Qin, X. Yu, S. Ji, FBW7-NRA41-SCD1 axis synchronously regulates apoptosis and ferroptosis in pancreatic cancer cells, Redox Biol. 38 (2021) 101807, https://doi.org/10.1016/j.redox.2020.101807.

[24] K. Iskandar, M. Rezlan, S.K. Yadav, C.H.J. Foo, G. Sethi, Y. Qiang, G.L. Bellot, S. Pervaiz, Synthetic lethality of a novel small molecule against mutant KRAS-expressing cancer cells involves AKT-dependent ROS production, Antioxidants Redox Signal. 24 (2015) 781–794, https://doi.org/10.1089/ars.2015.6362.

[25] E. Dai, L. Han, J. Liu, Y. Xie, H.J. Zeh, R. Kang, L. Bai, D. Tang, Ferroptotic damage promotes pancreatic tumorigenesis through a TMEM173/STING-dependent DNA sensor pathway, Nat. Commun. 11 (2020) 6339, https://doi.org/10.1038/s41467-020-20154-8.

[26] X. Chen, R. Kang, G. Kroemer, D. Tang, Targeting ferroptosis in pancreatic cancer: a double-edged sword, Trends in Cancer 7 (2021) 891–901, https://doi.org/10.1016/j.trecan.2021.04.005.

[27] J. Lu, A. Holmgren, Selenoproteins, J. Biol. Chem. 284 (2009) 723–727, https://doi.org/10.1074/jbc.R800045200.

[28] V.K. Wandt, N. Winkelbeiner, J. Bornhorst, B. Witt, S. Raschke, L. Simon, F. Ebert, A.P. Kipp, T. Schwerdtle, A matter of concern – trace element dyshomeostasis and genomic stability in neurons, Redox Biol. 41 (2021), 101877, https://doi.org/10.1016/j.redox.2021.101877.

[29] A.P. Nogara, M. Bortoli, L. Orian, B.T.J. Rocha, Biological activity of synthetic organoselenium compounds: what do we know about the mechanism? Curr. Chem. Biol. 16 (2022) 12–24, https://doi.org/10.2174/2212796816666220422135204.

[30] A. Daiber, F. Di Lisa, S. Lamas, Virtual issue by COST Action BM1203 (EU-ROS) "Emerging concepts in redox biology and oxidative stress,", Redox Biol. 8 (2016) 439–441, https://doi.org/10.1016/j.redox.2015.12.007.

[31] A.P. Fernandes, V. Gandin, Selenium compounds as therapeutic agents in cancer, Biochim. Biophys. Acta Gen. Subj. 1850 (2015) 1642–1660, https://doi.org/10.1016/j.bbagen.2014.10.008.

[32] N. Lee, S.J. Park, M. Lange, T. Tseyang, M.B. Doshi, T.Y. Kim, Y. Song, D.I. Kim, P. L. Greer, J.A. Olzmann, J.B. Spinelli, D. Kim, Selenium reduction of ubiquinone via SQOR suppresses ferroptosis, bioRxiv (2023), https://doi.org/10.1101/2023.04.13.535674, 2023.04.13.535674.

[33] M. Conrad, B. Proneth, Selenium: tracing another essential element of ferroptotic cell death, Cell Chem. Biol. 27 (2020) 409–419, https://doi.org/10.1016/j.chembiol.2020.03.012.

[34] Z. Li, L. Ferguson, K.K. Deol, M.A. Roberts, L. Magtanong, J.M. Hendricks, G. A. Mousa, S. Kilinc, K. Schaefer, J.A. Wells, M.C. Bassik, A. Goga, S.J. Dixon, N. T. Ingolia, J.A. Olzmann, Ribosome stalling during selenoprotein translation exposes a ferroptosis vulnerability, Nat. Chem. Biol. 18 (2022) 751–761, https://doi.org/10.1038/s41589-022-01033-3.

[35] I. Ingold, C. Berndt, S. Schmitt, S. Doll, G. Poschmann, K. Buday, A. Roveri, X. Peng, F. Porto Freitas, T. Seibt, L. Mehr, M. Aichler, A. Walch, D. Lamp, M. Jastroch, S. Miyamoto, W. Wurst, F. Ursini, E.S.J. Arnér, N. Fradejas-Villar, U. Schweizer, H. Zischka, J.P. Friedmann Angeli, M. Conrad, Selenium utilization by GPX4 is required to prevent hydroperoxide-induced ferroptosis, Cell 172 (2018) 409–422.e21, https://doi.org/10.1016/j.cell.2017.11.048.

[36] C.S.R. Jankowski, J.D. Rabinowitz, Selenium modulates cancer cell response to pharmacologic ascorbate, Cancer Res. 82 (2022) 3486–3498, https://doi.org/10.1158/0008-5472.CAN-22-0408.

[37] N.E. Mbah, C.A. Lyssiotis, Metabolic regulation of ferroptosis in the tumor microenvironment, J. Biol. Chem. 298 (2022), 101617, https://doi.org/10.1016/j.jbc.2022.101617.

[38] A. Carrer, S. Trefely, S. Zhao, S. Campbell, R.J. Norgard, K.C. Schultz, S. Sidoli, J.L. D. Parris, H.C. Affronti, S. Sivanand, S. Egolf, Y. Sela, M. Trizzino, J. Gardini, B. A. Garcia, N.W. Snyder, B.Z. Stanger, K. Wellen, Acetyl-CoA Metabolism Supports Multi-step Pancreatic Tumorigenesis, Cancer Discov, 2019, https://doi.org/10.1158/2159-8290.CD-18-0567. CD-18-0567.

[39] J.W. Clendening, L.Z. Penn, Targeting tumor cell metabolism with statins, Oncogene 31 (2012) 4967, https://doi.org/10.1038/onc.2012.6.

[40] G.H. McGregor, A.D. Campbell, S.K. Fey, S. Tumanov, D. Sumpton, G.R. Blanco, G. Mackay, C. Nixon, A. Vazquez, O.J. Sansom, J.J. Kamphorst, Targeting the metabolic response to statin-mediated oxidative stress produces a synergistic antitumor response, Cancer Res. 80 (2020) 175–188, https://doi.org/10.1158/0008-5472.CAN-19-0644.

[41] K. Bersuker, J.M. Hendricks, Z. Li, L. Magtanong, B. Ford, P.H. Tang, M.A. Roberts, B. Tong, T.J. Maimone, R. Zoncu, M.C. Bassik, D.K. Nomura, J.A. Olzmann, The CoQ oxidoreductase FSP1 acts parallel to GPX4 to inhibit ferroptosis, Nature 575 (2019) 688–692, https://doi.org/10.1038/s41586-019-1705-2.

[42] C. Mao, X. Liu, Y. Zhang, G. Lei, Y. Yan, H. Lee, P. Koppula, S. Wu, L. Zhuang, B. Fang, M. V Poyurovsky, K. Olszewski, B. Gan, DHODH-mediated ferroptosis defence is a targetable vulnerability in cancer, Nature 593 (2021) 586–590, https://doi.org/10.1038/s41586-021-03539-7.

[43] S. Deshwal, M. Onishi, T. Tatsuta, T. Bartsch, E. Cors, K. Ried, K. Lemke, H. Nolte, P. Giavalisco, T. Langer, Mitochondria regulate intracellular coenzyme Q transport and ferroptotic resistance via STARD7, Nat. Cell Biol. 25 (2023) 246–257, https://doi.org/10.1038/s41556-022-01071-y.

[44] L. Arslanbaeva, G. Tosi, M. Ravazzolo, M. Simonato, F.A. Tucci, S. Pece, P. Cogo, M.M. Santoro, UBIAD1 and CoQ10 protect melanoma cells from lipid peroxidation-mediated cell death, Redox Biol. 51 (2022), 102272, https://doi.org/10.1016/j.redox.2022.102272.

[45] J. Li, K.T. Byrne, F. Yan, E.J. Wherry, R.H. Vonderheide, B.Z. Stanger, J. Li, K. T. Byrne, F. Yan, T. Yamazoe, Z. Chen, T. Baslan, L.P. Richman, Tumor cell-intrinsic factors underlie heterogeneity of immune cell infiltration and response to article tumor cell-intrinsic factors underlie heterogeneity of immune cell infiltration and response to immunotherapy, Immunity 49 (2018) 178–193.e7, https://doi.org/10.1016/j.immuni.2018.06.006.

[46] D. Krasowska, F. Begini, C. Santi, F. Mangiavacchi, J. Drabowicz, L. Sancineto, Ultrasound-assisted synthesis of alkali metals diselenides (M_2Se_2) and their application for the gram-scale preparation of 2,2'-diselenobis(benzoic acid), ARKIVOC (Gainesville, FL, U. S.) (2019) 24–37, https://doi.org/10.24820/ark.5550190.p010.981, 2019.

[47] V. Nascimento, P.S. Cordeiro, M. Arca, F. Marini, L. Sancineto, A.L. Braga, V. Lippolis, M. Iwaoka, C. Santi, Fast and easy conversion of ortho amidoaryldiselenides into the corresponding ebselen-like derivatives driven by theoretical investigations, New J. Chem. 44 (2020) 9444–9451, https://doi.org/10.1039/D0NJ01605E.

[48] C. Santi, S. Santoro, B. Battistelli, L. Testaferri, M. Tiecco, Preparation of the First bench-stable phenyl selenolate: an interesting "on water" nucleophilic reagent, Eur. J. Org Chem. (2008) 5387–5390, https://doi.org/10.1002/ejoc.200800869, 2008.

[49] M. Dorsch, M. Kowalczyk, M. Planque, G. Heilmann, S. Urban, P. Dujardin, J. Forster, K. Ueffing, S. Nothdurft, S. Oeck, A. Paul, S.T. Liffers, F. Kaschani, M. Kaiser, A. Schramm, J.T. Siveke, M.M. Winslow, S.-M. Fendt, P. Nalbant, B. M. Grüner, Statins affect cancer cell plasticity with distinct consequences for tumor progression and metastasis, Cell Rep. 37 (2021), 110056, https://doi.org/10.1016/j.celrep.2021.110056.

[50] I. Kaymak, C.R. Maier, W. Schmitz, A.D. Campbell, B. Dankworth, C.P. Ade, S. Walz, M. Paauwe, C. Kalogirou, H. Marouf, M.T. Rosenfeldt, D.M. Gay, G. H. McGregor, O.J. Sansom, A. Schulze, Mevalonate pathway provides ubiquinone to maintain pyrimidine synthesis and survival in p53-deficient cancer cells exposed to metabolic stress, Cancer Res. 80 (2020) 189, https://doi.org/10.1158/0008-5472.CAN-19-0650. LP – 203.

[51] G. Miotto, M. Rossetto, M.L. Di Paolo, L. Orian, R. Venerando, A. Roveri, A.-M. Vučković, V. Bosello Travain, M. Zaccarin, L. Zennaro, M. Maiorino, S. Toppo, F. Ursini, G. Cozza, Insight into the mechanism of ferroptosis inhibition by ferrostatin-1, Redox Biol. 28 (2020), 101328, https://doi.org/10.1016/j.redox.2019.101328.

[52] C. Santi, C. Scimmi, L. Sancineto, Ebselen and analogues: pharmacological properties and synthetic strategies for their preparation, Molecules 26 (2021), https://doi.org/10.3390/molecules26144230.

[53] M. Santi, V. Frusca, M.L. Ermini, A.K. Mapanao, P. Sarogni, A. Gonnelli, N. Giannini, A. Zamborlin, L. Biancalana, F. Marchetti, V. Voliani, Hybrid nano-architectures loaded with metal complexes for the co-chemotherapy of head and neck carcinomas, J. Mater. Chem. B 11 (2023) 325–334, https://doi.org/10.1039/D2TB01930B.

[54] D. Cassano, M. Summa, S. Pocoví-Martínez, A.-K. Mapanao, T. Catelani, R. Bertorelli, V. Voliani, Biodegradable ultrasmall-in-nano gold architectures: mid-period in vivo distribution and excretion assessment, part, Part. Syst. Charact. 36 (2019), 1800464, https://doi.org/10.1002/ppsc.201800464.

[55] P. Sarogni, A.K. Mapanao, A. Gonnelli, M.L. Ermini, S. Marchetti, C. Kusmic, F. Paiar, V. Voliani, Chorioallantoic membrane tumor models highlight the effects of cisplatin compounds in oral carcinoma treatment, iScience 25 (2022), 103980, https://doi.org/10.1016/j.isci.2022.103980.

[56] L. Galluzzi, I. Vitale, S.A. Aaronson, J.M. Abrams, D. Adam, P. Agostinis, E. S. Alnemri, L. Altucci, I. Amelio, D.W. Andrews, M. Annicchiarico-Petruzzelli, A. V Antonov, E. Arama, E.H. Baehrecke, N.A. Barlev, N.G. Bazan, F. Bernassola, M.J. M. Bertrand, K. Bianchi, M. V Blagosklonny, K. Blomgren, C. Borner, P. Boya, C. Brenner, M. Campanella, E. Candi, D. Carmona-Gutierrez, F. Cecconi, F.K.-M. Chan, N.S. Chandel, E.H. Cheng, J.E. Chipuk, J.A. Cidlowski, A. Ciechanover, G. M. Cohen, M. Conrad, J.R. Cubillos-Ruiz, P.E. Czabotar, V. D'Angiolella, T. M. Dawson, V.L. Dawson, V. De Laurenzi, R. De Maria, K.-M. Debatin, R. J. DeBerardinis, M. Deshmukh, N. Di Daniele, F. Di Virgilio, V.M. Dixit, S.J. Dixon, C.S. Duckett, B.D. Dynlacht, W.S. El-Deiry, J.W. Elrod, G.M. Fimia, S. Fulda, A. J. García-Sáez, A.D. Garg, C. Garrido, E. Gavathiotis, P. Golstein, E. Gottlieb, D. R. Green, L.A. Greene, H. Gronemeyer, A. Gross, G. Hajnoczky, J.M. Hardwick, I. S. Harris, M.O. Hengartner, C. Hetz, H. Ichijo, M. Jäättelä, B. Joseph, P.J. Jost, P. P. Juin, W.J. Kaiser, M. Karin, T. Kaufmann, O. Kepp, A. Kimchi, R.N. Kitsis, D. J. Klionsky, R.A. Knight, S. Kumar, S.W. Lee, J.J. Lemasters, B. Levine, A. Linkermann, S.A. Lipton, R.A. Lockshin, C. López-Otín, S.W. Lowe, T. Luedde, E. Lugli, M. MacFarlane, F. Madeo, M. Malewicz, W. Malorni, G. Manic, J.-C. Marine, S.J. Martin, J.-C. Martinou, J.P. Medema, P. Mehlen, P. Meier, S. Melino, E.A. Miao, J.D. Molkentin, U.M. Moll, C. Muñoz-Pinedo, S. Nagata, G. Nuñez, A. Oberst, M. Oren, M. Overholtzer, M. Pagano, T. Panaretakis, M. Pasparakis, J.M. Penninger, D.M. Pereira, S. Pervaiz, M.E. Peter, M. Piacentini, P. Pinton, J.H.M. Prehn, H. Puthalakath, G.A. Rabinovich, M. Rehm, R. Rizzuto, C. M.P. Rodrigues, D.C. Rubinsztein, T. Rudel, K.M. Ryan, E. Sayan, L. Scorrano, F. Shao, Y. Shi, J. Silke, H.-U. Simon, A. Sistigu, B.R. Stockwell, A. Strasser, G. Szabadkai, S.W.G. Tait, D. Tang, N. Tavernarakis, A. Thorburn, Y. Tsujimoto, B. Turk, T. Vanden Berghe, P. Vandenabeele, M.G. Vander Heiden, A. Villunger, H. W. Virgin, K.H. Vousden, D. Vucic, E.F. Wagner, H. Walczak, D. Wallach, Y. Wang, J.A. Wells, W. Wood, J. Yuan, Z. Zakeri, B. Zhivotovsky, L. Zitvogel, G. Melino, G. Kroemer, Molecular mechanisms of cell death: recommendations of the nomenclature committee on cell death 2018, Cell Death Differ. 25 (2018) 486–541, https://doi.org/10.1038/s41418-017-0012-4.

[57] A.M. Lamade, L. Wu, H.H. Dar, H.L. Mentrup, I.H. Shrivastava, M.W. Epperly, C. M. St Croix, Y.Y. Tyurina, T.S. Anthonymuthu, Q. Yang, A.A. Kapralov, Z. Huang, G. Mao, A.A. Amoscato, Z.E. Hier, M.A. Artyukhova, G. Shurin, J.C. Rosenbaum, P. J. Gough, J. Bertin, A.P. VanDemark, S.C. Watkins, K.P. Mollen, I. Bahar, J. S. Greenberger, V.E. Kagan, M.J. Whalen, H. Bayır, Inactivation of RIP3 kinase sensitizes to 15LOX/PEBP1-mediated ferroptotic death, Redox Biol. 50 (2022), 102232, https://doi.org/10.1016/j.redox.2022.102232.

[58] D.R. Richardson, D.J.R. Lane, E.M. Becker, M.L.-H. Huang, M. Whitnall, Y. S. Rahmanto, A.D. Sheftel, P. Ponka, Mitochondrial iron trafficking and the integration of iron metabolism between the mitochondrion and cytosol, Proc. Natl. Acad. Sci. USA 107 (2010) 10775–10782, https://doi.org/10.1073/pnas.0912925107.

[59] D.M. Ward, S.M. Cloonan, Mitochondrial iron in human Health and disease, Annu. Rev. Physiol. 81 (2019) 453–482. 10.1146/annurev-physiol-020518-114742.

[60] H.O. Fearnhead, P. Vandenabeele, T. Vanden Berghe, How do we fit ferroptosis in the family of regulated cell death? Cell Death Differ. 24 (2017) 1991–1998, https://doi.org/10.1038/cdd.2017.149.

[61] S.J. Dixon, Ferroptosis: bug or feature? Immunol. Rev. 277 (2017) 150–157, https://doi.org/10.1111/imr.12533.

[62] S. Nagdas, J.A. Kashatus, A. Nascimento, S.S. Hussain, R.E. Trainor, S.R. Pollock, S. J. Adair, A.D. Michaels, H. Sesaki, E.B. Stelow, T.W. Bauer, D.F. Kashatus, Drp1 promotes KRas-driven metabolic changes to drive pancreatic tumor growth, Cell Rep. 28 (2019) 1845–1859.e5, https://doi.org/10.1016/j.celrep.2019.07.031.

[63] F. Weinberg, R. Hamanaka, W.W. Wheaton, S. Weinberg, J. Joseph, M. Lopez, B. Kalyanaraman, G.M. Mutlu, G.R.S. Budinger, N.S. Chandel, Mitochondrial metabolism and ROS generation are essential for Kras-mediated tumorigenicity, Proc. Natl. Acad. Sci. USA 107 (2010) 8788, https://doi.org/10.1073/pnas.1003428107. LP – 8793.

[64] J.J. Kamphorst, J.R. Cross, J. Fan, E. de Stanchina, R. Mathew, E.P. White, C. B. Thompson, J.D. Rabinowitz, Hypoxic and Ras-transformed cells support growth by scavenging unsaturated fatty acids from lysophospholipids, Proc. Natl. Acad. Sci. USA 110 (2013) 8882–8887, https://doi.org/10.1073/pnas.1307237110.

[65] K. Shimada, R. Skouta, A. Kaplan, W.S. Yang, M. Hayano, S.J. Dixon, L.M. Brown, C.A. Valenzuela, A.J. Wolpaw, B.R. Stockwell, Global survey of cell death mechanisms reveals metabolic regulation of ferroptosis, Nat. Chem. Biol. 12 (2016) 497–503, https://doi.org/10.1038/nchembio.2079.

[66] V.S. Viswanathan, M.J. Ryan, H.D. Dhruv, S. Gill, O.M. Eichhoff, B. Seashore-Ludlow, S.D. Kaffenberger, J.K. Eaton, K. Shimada, A.J. Aguirre, S.R. Viswanathan, S. Chattopadhyay, P. Tamayo, W.S. Yang, M.G. Rees, S. Chen, Z. V Boskovic, S. Javaid, C. Huang, X. Wu, Y.-Y. Tseng, E.M. Roider, D. Gao, J.M. Cleary, B. M. Wolpin, J.P. Mesirov, D.A. Haber, J.A. Engelman, J.S. Boehm, J.D. Kotz, C. S. Hon, Y. Chen, W.C. Hahn, M.P. Levesque, J.G. Doench, M.E. Berens, A.F. Shamji, P.A. Clemons, B.R. Stockwell, S.L. Schreiber, Dependency of a therapy-resistant state of cancer cells on a lipid peroxidase pathway, Nature 547 (2017) 453–457, https://doi.org/10.1038/nature23007.

[67] P.J. Mullen, R. Yu, J. Longo, M.C. Archer, The interplay between cell signalling and the mevalonate pathway in cancer, Nat. Publ. Gr. 16 (2016) 718–731, https://doi.org/10.1038/nrc.2016.76.

[68] X. Yao, R. Xie, Y. Cao, J. Tang, Y. Men, H. Peng, W. Yang, Simvastatin induced ferroptosis for triple-negative breast cancer therapy, J. Nanobiotechnol. 19 (2021) 311, https://doi.org/10.1186/s12951-021-01058-1.

[69] S.A. Kerk, L. Lin, A.L. Myers, D.J. Sutton, A. Andren, P. Sajjakulnukit, L. Zhang, Y. Zhang, J.A. Jiménez, B.S. Nelson, B. Chen, A. Robinson, G. Thurston, S.B. Kemp, N.G. Steele, M.T. Hoffman, H.-J. Wen, D. Long, S.E. Ackenhusen, J. Ramos, X. Gao, Z.C. Nwosu, S. Galban, C.J. Halbrook, D.B. Lombard, D.R. Piwnica-Worms, H. Ying, M. Pasca di Magliano, H.C. Crawford, Y.M. Shah, C.A. Lyssiotis, Metabolic requirement for GOT2 in pancreatic cancer depends on environmental context, Elife 11 (2022), e73245, https://doi.org/10.7554/eLife.73245.

[70] D.Y. Gui, L.B. Sullivan, A. Luengo, A.M. Hosios, L.N. Bush, N. Gitego, S. M. Davidson, E. Freinkman, C.J. Thomas, M.G. Vander Heiden, Environment dictates dependence on mitochondrial complex I for NAD+ and aspartate production and determines cancer cell sensitivity to metformin, Cell Metabol. 24 (2016) 716–727, https://doi.org/10.1016/j.cmet.2016.09.006.

[71] S. Jang, X.R. Chapa-Dubocq, Y.Y. Tyurina, C.M. St Croix, A.A. Kapralov, V. A. Tyurin, H. Bayır, V.E. Kagan, S. Javadov, Elucidating the contribution of mitochondrial glutathione to ferroptosis in cardiomyocytes, Redox Biol. 45 (2021), 102021, https://doi.org/10.1016/j.redox.2021.102021.

[72] J.P. Friedmann Angeli, M. Schneider, B. Proneth, Y.Y. Tyurina, V.A. Tyurin, V. J. Hammond, N. Herbach, M. Aichler, A. Walch, E. Eggenhofer, D. Basavarajappa, O. Rådmark, S. Kobayashi, T. Seibt, H. Beck, F. Neff, I. Esposito, R. Wanke, H. Förster, O. Yefremova, M. Heinrichmeyer, G.W. Bornkamm, E.K. Geissler, S. B. Thomas, B.R. Stockwell, V.B. O'Donnell, V.E. Kagan, J.A. Schick, M. Conrad, Inactivation of the ferroptosis regulator Gpx4 triggers acute renal failure in mice, Nat. Cell Biol. 16 (2014) 1180–1191, https://doi.org/10.1038/ncb3064.

[73] N.P. Mena, P.J. Urrutia, F. Lourido, C.M. Carrasco, M.T. Núñez, Mitochondrial iron homeostasis and its dysfunctions in neurodegenerative disorders, Mitochondrion 21 (2015) 92–105, https://doi.org/10.1016/j.mito.2015.02.001.

[74] M. Gao, J. Yi, J. Zhu, A.M. Minikes, P. Monian, C.B. Thompson, X. Jiang, Role of mitochondria in ferroptosis, Mol. Cell. 73 (2019) 354–363.e3, https://doi.org/10.1016/j.molcel.2018.10.042.

[75] S. Javadov, Mitochondria and ferroptosis, Curr. Opin. Physiol. 25 (2022), 100483, https://doi.org/10.1016/j.cophys.2022.100483.

[76] T.M. Buscagan, J.T. Kaiser, D.C. Rees, Selenocyanate derived Se-incorporation into the nitrogenase Fe protein cluster, Elife 11 (2022), e79311, https://doi.org/10.7554/eLife.79311.

[77] B. Zheng, X.-D. Chen, S.-L. Zheng, R.H. Holm, Selenium as a structural surrogate of sulfur: template-assisted assembly of five types of tungsten–iron–sulfur/selenium clusters and the structural fate of chalcogenide reactants, J. Am. Chem. Soc. 134 (2012) 6479–6490, https://doi.org/10.1021/ja3010539.

[78] N. Spiller, V.G. Chilkuri, S. DeBeer, F. Neese, Sulfur vs. Selenium as bridging ligand in di-iron complexes: a theoretical analysis, Eur. J. Inorg. Chem. (2020) 1525–1538, https://doi.org/10.1002/ejic.202000033, 2020.

[79] V. Gandin, P. Khalkar, J. Braude, A.P. Fernandes, Organic selenium compounds as potential chemotherapeutic agents for improved cancer treatment, Free Radic. Biol. Med. 127 (2018) 80–97, https://doi.org/10.1016/j.freeradbiomed.2018.05.001.

[80] D. Bartolini, J. Commodi, M. Piroddi, L. Incipini, L. Sancineto, C. Santi, F. Galli, Glutathione S-transferase pi expression regulates the Nrf2-dependent response to hormetic diselenides, Free Radic. Biol. Med. 88 (2015) 466–480, https://doi.org/10.1016/j.freeradbiomed.2015.06.039.

[81] D. Krasowska, N. Iraci, C. Santi, J. Drabowicz, M. Cieslak, J. Kaźmierczak-Barańska, M. Palomba, K. Królewska-Golińska, J. Magiera, L. Sancineto, Diselenides and benzisoselenazolones as antiproliferative agents and glutathione-S-transferase inhibitors, Molecules 24 (2019), https://doi.org/10.3390/molecules24162914.